symmetry

MDPI

Article

Nuclear Structure Evolution Reflected from Local Relations

Man Bao * and Qian Wei

Department of Physics, University of Shanghai for Science and Technology, Shanghai 200093, China; 192262028@st.usst.edu.cn

* Correspondence: mbao@usst.edu.cn

Abstract: The structure evolution of nuclei which are in connection with symmetry breaking is one of the important problems not only for nuclear structures, but also for astrophysics and the spectroscopy of exotic nuclei. Many physical quantities can provide useful information of a shell structure, such as nuclear masses and nuclear charge radii. This paper introduces three kinds of local relations, i.e., the N_pN_n scheme respectively for the quadrupole deformation parameter and the excitation energy of the first 2^+, 4^+, 6^+ states, the $(\alpha N'_n + N'_p)$ relation for nuclear charge radii and α decay energies, and the so-called "nonpairing" relation for binding energies and nuclear charge radii. All these relations reflect the evolution of nuclear structures, involving shells, subshells, shape coexistence, phase transition and the Wigner effect. Some results from different models can be verified with each other.

Keywords: nuclear structure evolution; local relations; quadrupole deformation parameter; the excitation energy; nuclear charge radius; α decay energy; binding energy

Citation: Bao, M.; Wei, Q. Nuclear Structure Evolution Reflected from Local Relations. *Symmetry* **2021**, *13*, 2253. https://doi.org/10.3390/sym13122253

Academic Editors: Jorge Segovia, Yu-Gang Ma, De-Qing Fang and Fu-Rong Xu

Received: 1 October 2021
Accepted: 18 November 2021
Published: 26 November 2021

1. Introduction

The shell structure is found in many physical systems, such as atoms and nuclei. In the early 1930s, Bartlett discovered certain regularities in the composition of atomic nuclei and speculated that nucleons within nuclei might have their own shell structure [1–3]. Subsequently, more systematic studies were conducted by Elsasser, and it was found experimentally that some properties of the nucleus present obvious periodic changes as the number of protons or neutrons increase, and nuclei with several special proton or neutron numbers are particularly stable [4–6]. These special numbers are called "magic numbers", and were explained successfully by Mayer [7–9] and Jensen et al. [10–14] through introducing spin-orbit coupling in the mean field. The nuclear shell model, which represents magic numbers as well as experimental phenomena, such as spin, parity, magnetic moment and beta decay, was successfully developed through this line [15], and was proved to be very useful in studying the low-lying states of nuclei [16–18].

Nuclear mass (or binding energy) is a fundamental quantity of an atomic nucleus, and its measurement played an important role in the building of the nuclear shell model [7–15]. The shell structure of a neutron (proton) can be determined effectively by the double-neutron (-proton) separation energies, for their sudden decrease at magic numbers. For the nuclei away from the stability line, the binding energy decreases, and they become weak-bounded open systems near the drip line. These unstable nuclei may have different magic numbers and systematic evolution of their structures, which is in connection with the symmetry breaking that may arise [19]. In the early years, research was focused on nuclei with a small mass number, due to the limited experimental conditions. Nowadays, more than 3000 nuclei are synthesized experimentally [20–22] and more information of the nuclear structure can be obtained.

The structure evolution of nuclei, which is directly reflected in the ground and low-lying states, is one of the advanced topics of nuclear structure, and is also involved in astrophysics and the spectroscopy of exotic nuclei. Recently, many efforts were made

toward describing and predicting physical quantities, which provide useful information of shell structure, such as nuclear masses, α-decay energies, nuclear charge radii and so on. Some of these works that give relations connecting physical quantities of several neighbor nuclei or reveal certain phenomenon in local regions are called "local" relations, for example, the Garvey–Kelson mass relations [23,24], relations connected with neutron–proton interactions [25–30], and the N_pN_n scheme [31–35]. In this paper, three kinds of local relations and corresponding information reflecting nuclear structure evolutions are introduced and discussed.

2. Local Relations

In this section, three kinds of local relations that can reflect nuclear structure evolutions are introduced, and the corresponding discussions are made.

2.1. The N_pN_n Scheme of the Quadrupole Deformation Parameter e_2 or the Excitation Energy $E_{2_1^+}$, $E_{4_1^+}$ and $E_{6_1^+}$

The N_pN_n scheme was described by Casten, where $E_{2_1^+}$, $E_{4_1^+}/E_{2_1^+}$ and $B(E2, 0_1^+ \rightarrow 2_1^+)$ for even–even nuclei exhibit smooth systematics against the product of valence proton number N_p and valence neutron number N_n [31,36,37]. It works equally well for the quadrupole deformation parameter e_2 (correlated with the intrinsic quadrupole moment) of all parity types of medium-heavy nuclei in Ref. [34].

In Figure 1, the absolute value of e_2 in the Nilsson perturbed–spheroid parameterization taken from Ref. [38] is presented versus N_pN_n for nuclei in three different regions [34]. Here only e_2 of nuclei with known experimental binding energies [22] are plotted. As discussed in Ref. [34], the correlation between e_2 and N_pN_n shown in Figure 1 is very compact, except for several anomalies which are labeled by the red circles in Figure 1a and marked by a red circle in Figure 1b,c.

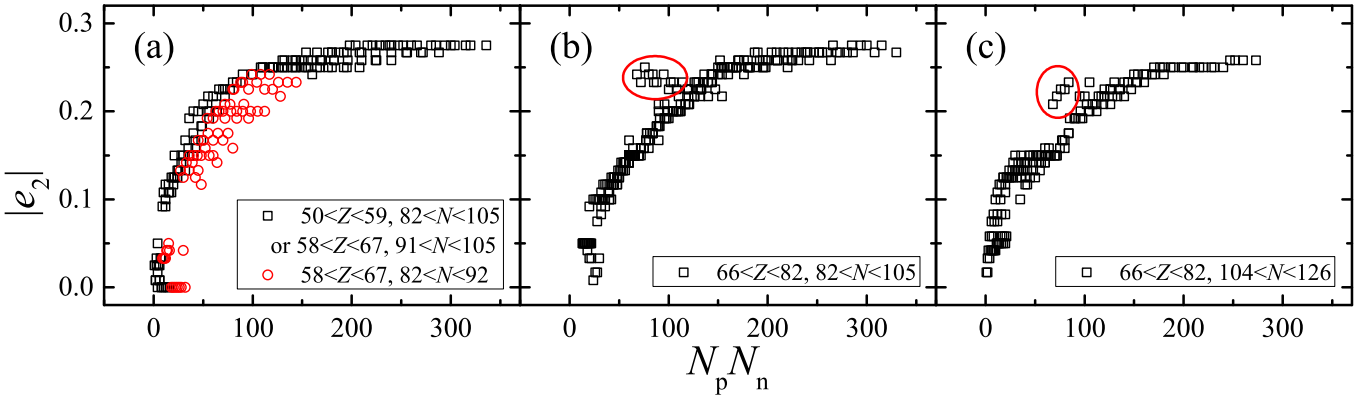

Figure 1. $|e_2|$ in the Nilsson perturbed–spheroid parametrization [38] versus N_pN_n. (**a**) For nuclei with $50 < Z < 67$ and $82 < N < 105$. (**b**) For nuclei with $66 < Z < 82$ and $82 < N < 105$. (**c**) For nuclei with $66 < Z < 82$ and $104 < N < 126$. The anomalies are labeled by the red circles in panel (**a**) and marked by a red circle in panels (**b**,**c**).

Affected by the $Z = 64$ subshell, the red circles in Figure 1a, which correspond to e_2 of nuclei with $58 < Z < 67$ and $82 < N < 92$, deviate from the other black squares [34]. In addition, e_2 of $N = 84$ isotones equals 0 as shown in Figure 1a, which is because these nuclei are soft and the difference between the equilibrium deformation and the expected value of the deformation is large [34].

Those anomalies in Figure 1b,c correspond to nuclei with $Z = 77$ or 78 and $N = 99 \sim 109$, which belong to a complex region where there exists large γ softness, deformation and transition [34]. In Ref. [35], similar anomalies are pointed out in the N_pN_n scheme for the excitation energy of the first 2^+ state $E_{2_1^+}$ of even–even nuclei with $Z = 78$ or 80 and $83 < N < 105$, based on the experimental data taken from Ref. [39] (see Figure 2a

with the anomalies labeled by the red circles). However, it is no longer obvious with the updated experimental data taken from Ref. [40], as shown in Figure 2b.

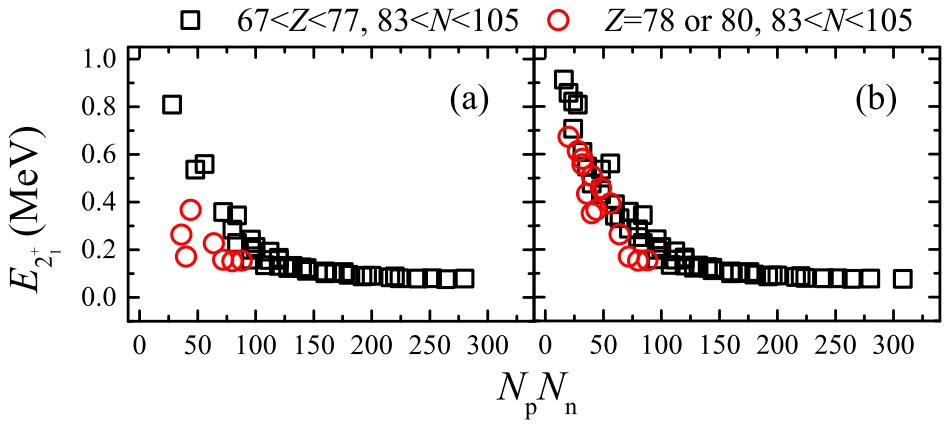

Figure 2. $E_{2_1^+}$ versus N_pN_n for even-even nuclei with $67 < Z < 81$ and $83 < N < 105$. The experimental data are taken from Ref. [39] for panel (**a**) [35] and Ref. [40] for panel (**b**), respectively. The red circles correspond to the $E_{2_1^+}$ of nuclei with $Z = 78$ or 80 and $83 < N < 105$.

In Ref. [41], e_2 is further discussed with the P factor, i.e., $N_pN_n/(N_p + N_n)$, in the same region of Figure 1b,c. $|e_2|$ in the Nilsson perturbed–spheroid parametrization [38] is plotted versus the P factor in Figure 3, where nuclei with $66 < Z < 76$ are labeled by black squares, and isotopes with $Z = 76 \sim 81$ are labeled by colored dots. With the increase in factor P, $|e_2|$ grows smoothly and becomes flat around $P \sim 6$ [41].

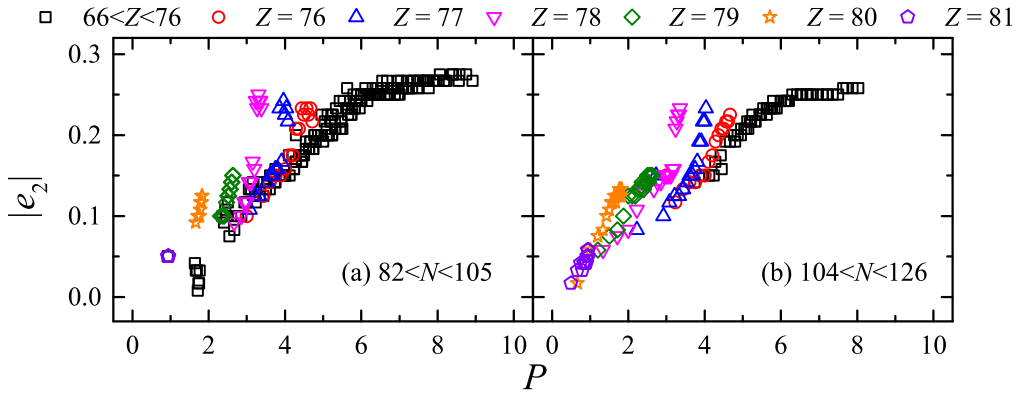

Figure 3. $|e_2|$ in the Nilsson perturbed–spheroid parametrization [38] versus the P factor. Panel (**a**,**b**) corresponds to $82 < N < 105$ and $104 < N < 126$, respectively. Nuclei with $66 < Z < 76$ are labeled by black squares, and isotopes with $Z = 76 \sim 81$ are labeled by red circles, blue up triangles, pink down triangles, green diamonds, orange stars and violet pentagons, respectively.

It is seen that some colored dots depart from black squares obviously. Most of these anomalies correspond to nuclei with $N = 97 \sim 104$ in Figure 3a and with $N = 105 \sim 109$ in Figure 3b, which near the midshell $N = 104$. This is explained by Ref. [41] that coexisting deformed states may descend into the low-lying spectrum for nuclei with $Z > 82$.

Similarly in Ref. [41], the relationship between $E_{2_1^+}$ [40] and the P factor is presented in Figure 4a for even–even nuclei with $67 < Z < 81$ and $83 < N < 105$. The black squares correspond to nuclei with $67 < Z < 75$, and isotopes with $Z = 76$, 78 and 80 are labeled by colored dots. It is obvious that the deviation between those colored dots and the black squares becomes larger with the increase in Z. This phenomenon also appears in the relation between $E_{4_1^+}$, $E_{6_1^+}$ [40] and the P factor, as shown in Figure 5a,c.

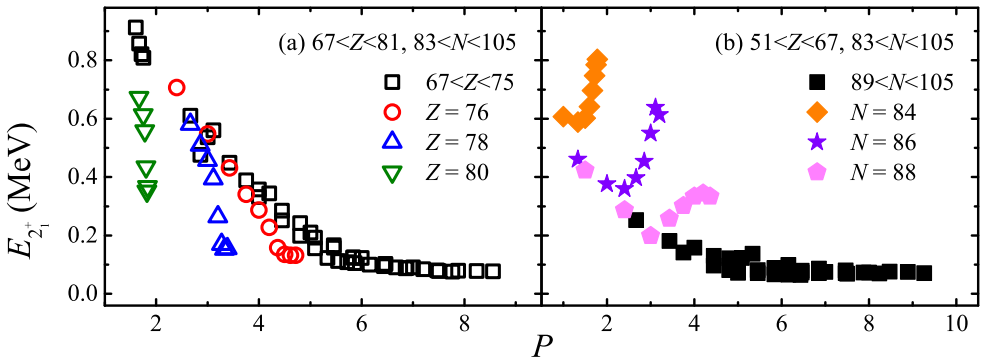

Figure 4. $E_{2_1^+}$[40] versus the P factor for even–even nuclei with $83 < N < 105$. Panels (**a**,**b**) correspond to nuclei with $67 < Z < 81$ and $51 < Z < 67$, respectively. The colored hollow dots in panel (**a**) are isotopes and the colored solid dots in panel (**b**) are isotones.

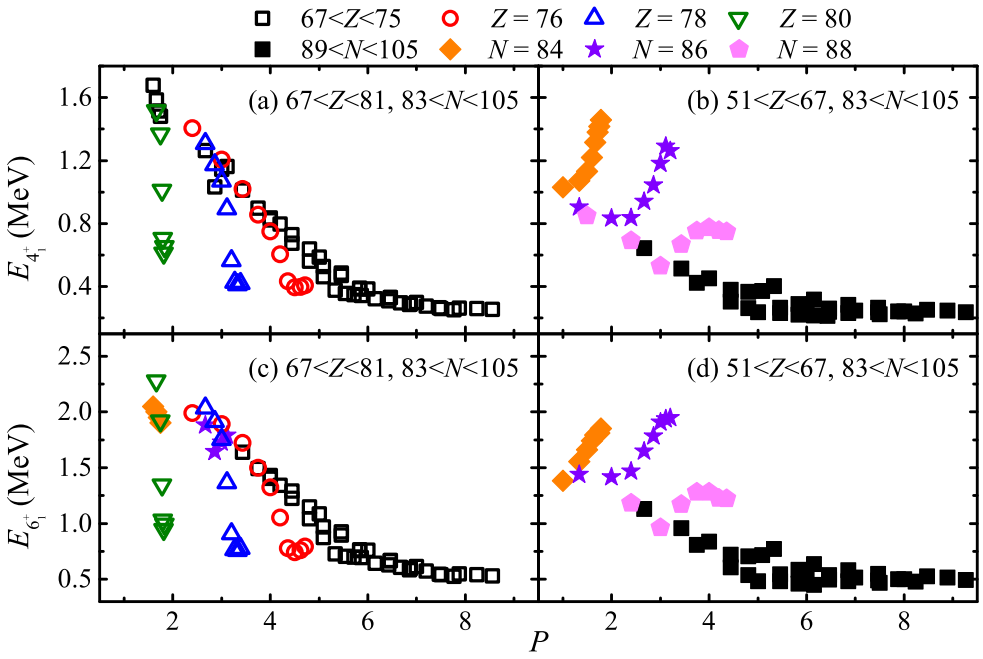

Figure 5. $E_{4_1^+}$ and $E_{6_1^+}$ [40] versus the P factor for even–even nuclei with $83 < N < 105$. Panels (**a**,**c**) correspond to nuclei with $67 < Z < 81$, while panels (**b**,**d**) correspond to nuclei with $51 < Z < 67$. The colored hollow dots are isotopes and the colored solid dots are isotones.

In addition, by comparing Figure 3 with Figure 1b,c, and Figure 4a with Figure 2b, it is easy to see that the anomalies for nuclei with $Z = 76 \sim 80$ are more conspicuous in the P factor plot than in the N_pN_n scheme for both $|e_2|$and $E_{2_1^+}$, and behave in a pattern with the proton number Z in the P factor plot [41] .

For even–even nuclei with $83 < N < 105$ and $51 < Z < 67$, $E_{2_1^+}$, $E_{4_1^+}$ and $E_{6_1^+}$ [40] are also plotted with the P factor in Figures 4b and 5b,d, respectively. It is seen that these excitation energies [40] of nuclei with $N = 84$, 86 and 88 (colored solid dots) are also deviated from the others (black solid dots) obviously, as well as those $N = 84$ and 86 isotones with $68 \leq Z \leq 74$ as shown in Figure 5c.

2.2. $(\alpha N'_n + N'_p)$ *Relation for Nuclear Charge Radii R and α Decay Energies* Q_α

It is shown in Ref. [42] that nuclear charge radii R have a good linear relationship with $(\alpha N'_n + N'_p)$ in a local region. Here, α is a fitting parameter, $N'_p = Z - Z_0$ and $N'_n = N - N_0$, where Z_0 and N_0 are the beginning proton number and neutron number of a local region, respectively. However, some anomalies exist in several local regions [42].

Suppose that $R(N,Z) = k(\alpha N'_n + N'_p) + C$ nuclear charge radii are plotted versus $(\alpha N'_n + N'_p)$ in Figures 6 and 7 for several different local regions which are pointed to have anomalies in Ref. [42]. Here, the experimental value of R is taken from the CR2013 database [43,44], and k, α, C are obtained by χ^2-fitting.

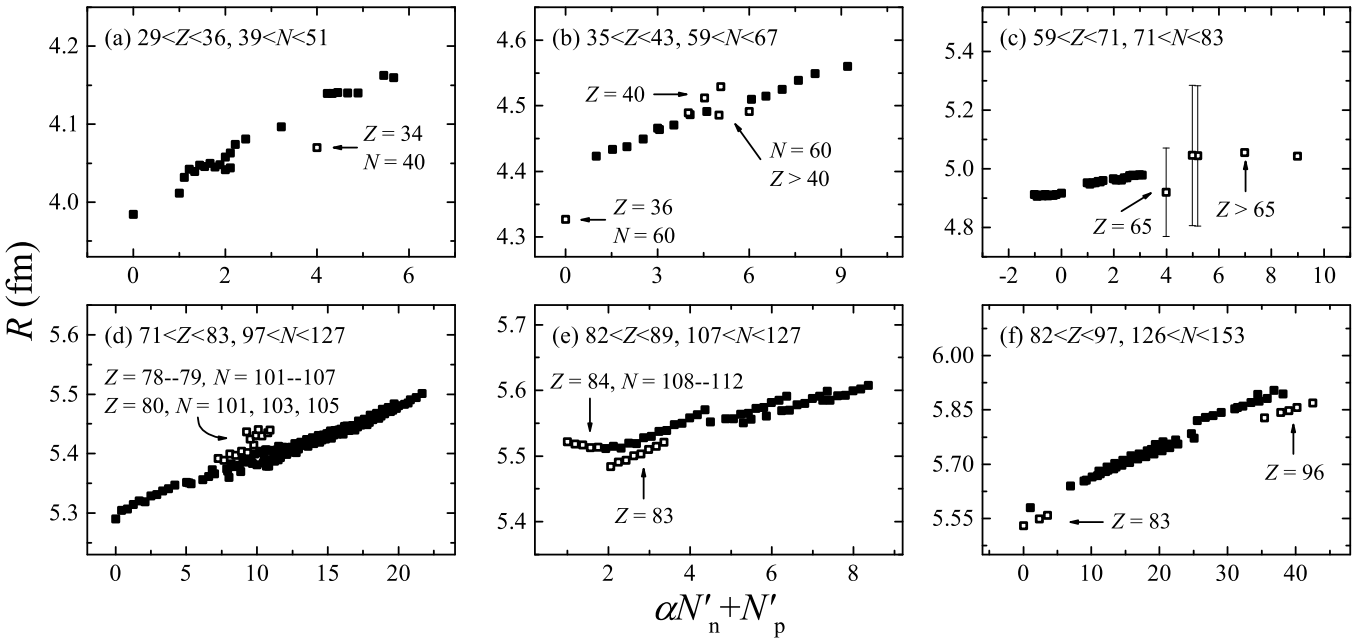

Figure 6. Nuclear charge radii R [43,44] versus $(\alpha N'_n + N'_p)$ in different regions. The anomalies are labeled by the open squares, and large experimental uncertainties (>0.15 fm) of R are shown in panel (**c**). The parameter α respectively equals 0.111, 0.534, −0.102, 0.417, 0.187 and 1.180 for panels (**a**–**f**).

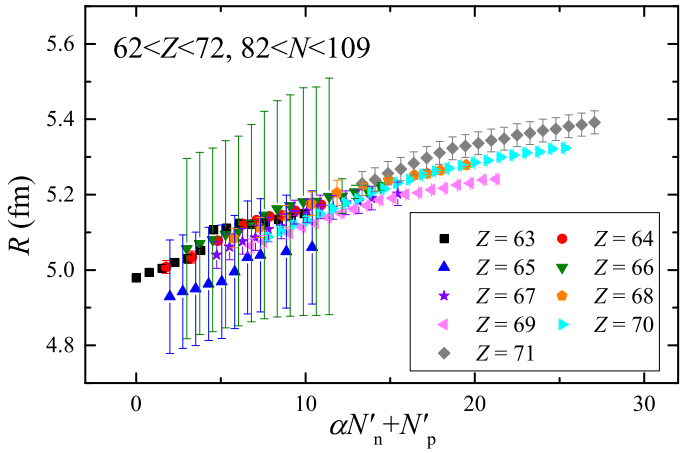

Figure 7. Nuclear charge radii R [43,44] versus $(\alpha N'_n + N'_p)$. Different symbols are used to label the chains of isotopes, and the experimental uncertainties of R are given. The parameter α is 0.763.

It is seen that nuclear charge radii of nuclei with $78 \leq Z \leq 80$ and $101 \leq N \leq 107$ in Figure 6d and of nuclei in Figure 7 also show abnormalities [42], which are generally consistent with the anomalies of $|e_2|$ and $E_{2_1^+}$, $E_{4_1^+}$, $E_{6_1^+}$ in the N_pN_n scheme and the P factor plot, as discussed in Section 2.1.

The anomalies given in Figure 6b may correspond to the phase transition at $N = 60$ and $Z \sim 40$ [45], where it is also explained by Ref. [46] that the sudden deformation here is contrasted with the deformation from a sphere to an ellipsoid.

As shown in Figures 6c and 7, R of nuclei with $Z = 65$ have very large experimental uncertainties (about 0.15 fm), which may lead to much lower positions in panels relative to

the others [42]. For the other anomalies presented in Figures 6a,e,f and 7, the structure of them should be further studied in the future.

The linear relationship between α decay energies Q_α and $(\alpha N_n + N_p)$ is also pointed out in Ref. [47]. In Figure 8, Q_α taken from Ref. [22] is plotted versus $(\alpha N'_n + N'_p)$ in four different regions, and those anomalies which deviate from the others (black dots) obviously are labeled by colored dots.

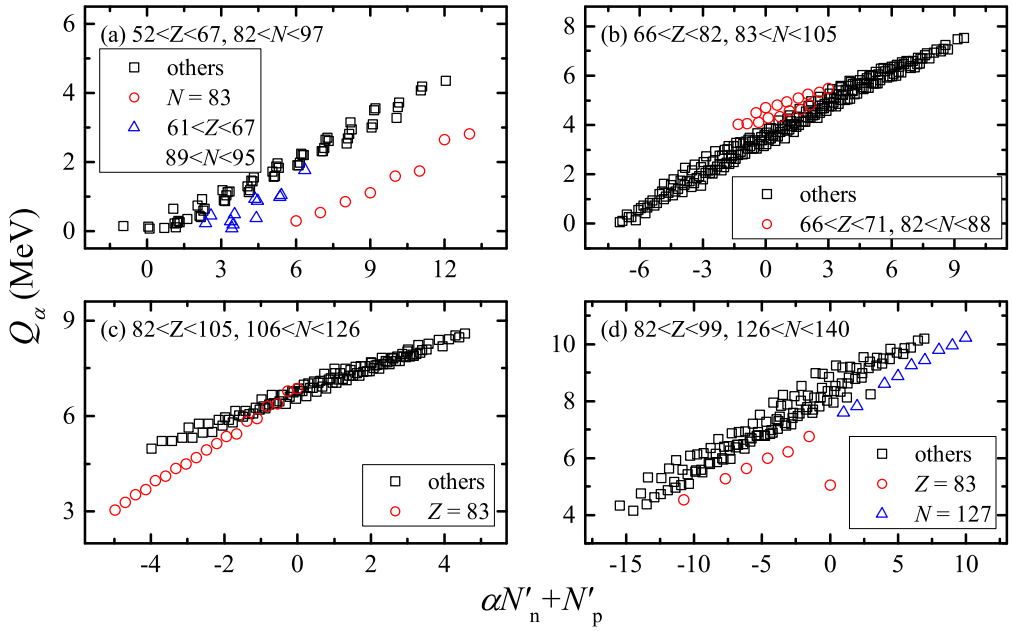

Figure 8. α decay energies Q_α[22] versus $(\alpha N'_n + N'_p)$ in different regions. The anomalies are labeled by colored dots. The parameter α respectively equals -0.947, -0.442, -0.277 and -1.539 for panels (**a**–**d**).

Blue triangles in Figure 8a correspond to nuclei with $Z \sim 64$ and $N \sim 90$, which may be influenced by the $Z = 64$ subshell [31,36,48–50]. The red circles in Figure 8b denote nuclei with $66 < Z < 71$ and $83 < N < 88$, which also exhibit an anomaly as shown in Figure 5b,d ($E_{4_1^+}$, $E_{6_1^+}$ versus the P factor) and Figure 7 (R versus $(\alpha N'_n + N'_p)$). The deviations of Q_α between $Z = 83$ isotopes and the others in Figure 8c,d are also reflected in Figure 6e,f.

2.3. The So-Called "Nonpairing" Relation of Binding Energies B and Nuclear Charge Radii R

The so-called "nonpairing" interaction between the last two protons δV_{pp} or the last two neutrons δV_{nn} are defined as follows:

$$-\delta V_{pp}(Z-1,Z;N) = \frac{1}{2}[B(N,Z) - B(N,Z-1) - B(N,Z-2) + B(N,Z-3)], \quad (1)$$

$$-\delta V_{nn}(N-1,N;Z) = \frac{1}{2}[B(N,Z) - B(N-1,Z) - B(N-2,Z) + B(N-3,Z)], \quad (2)$$

respectively [45]. $B(N,Z)$ is the binding energy of nuclei with neutron number N and proton number Z.

Based on the AME2020 database [22], δV_{pp} and δV_{nn} are calculated by using Equations (1) and (2), and are plotted versus Z and N, respectively, in Figure 9 [45]. Those blue circles or green tringles, which correspond to nuclei with $Z - N = 1$ or 2 for δV_{pp} and $N - Z = 1$ or 2 for δV_{nn}, are quite large, as shown in Figure 9a,b. This is mainly caused by the Wigner effect [45], which results from the neutron–proton correlation and is dependent on the isospin.

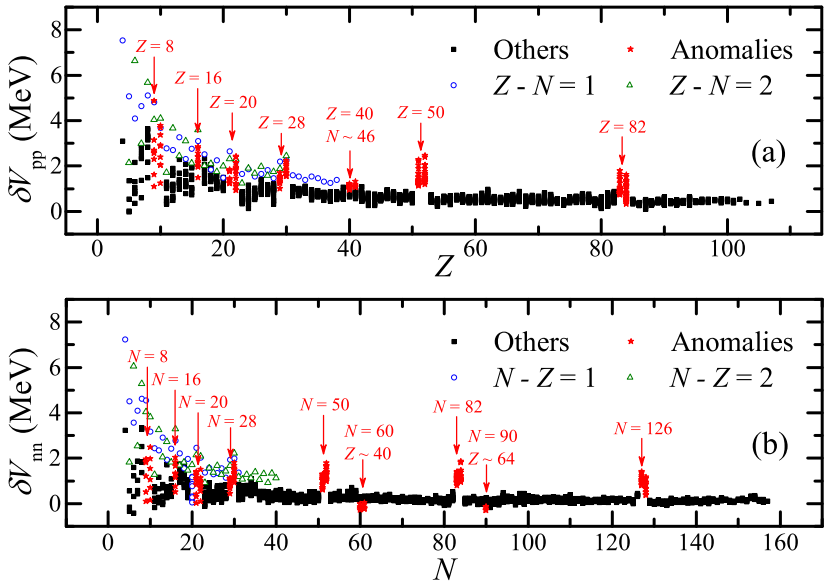

Figure 9. (**a**): $\delta V_{\rm pp}$ versus Z. (**b**): $\delta V_{\rm nn}$ versus N. The anomalies are labeled by the red stars. The blue circles and green triangles correspond to nuclei with $Z-N=1$ and $Z-N=2$ in panel (**a**), and those with $N-Z=1$ and $N-Z=2$ in panel (**b**).

The other anomalies that are irrelevant to the Wigner effect are labeled by the red circles in Figure 9. As pointed in Refs. [45,51,52], these anomalies are "fingerprints" of nuclear structure involving (sub-)shells and phase transitions.

New magic numbers $N, Z = 16$ discovered in Refs. [53,54] are represented in Figure 9a,b, respectively [45]. The $Z = 40$ subshell (for $N < 60$) [31,36,48,55,56] and $Z = 64$ subshell (for $N < 90$) [31,36,48–50] correspond to anomalies with $Z = 40$, $N \sim 56$ of $\delta V_{\rm pp}$ and $Z \sim 64$, $N = 90$ of $\delta V_{\rm nn}$, respectively [45]. In addition, the phase transition at $N = 60$ and $Z \sim 40$ also behaves abnormally as shown in Figure 9b [45].

Similar to $\delta V_{\rm nn}$ discussed above, $\delta R_{\rm nn}$ is defined in Ref. [42], i.e.,

$$\delta R_{\rm nn}(N,Z) = R(N,Z) - R(N-1,Z) - R(N-2,Z) + R(N-3,Z). \quad (3)$$

Here, $R(N,Z)$ is the nuclear charge radii of nuclei with neutron number N and proton number Z. Based on the CR2013 database [43,44], $\delta R_{\rm nn}$ is calculated and plotted versus the neutron number N in Figure 10 [42]. The red dash lines of $\delta R_{\rm nn} = \pm 0.03$ fm are plotted to guide the eyes.

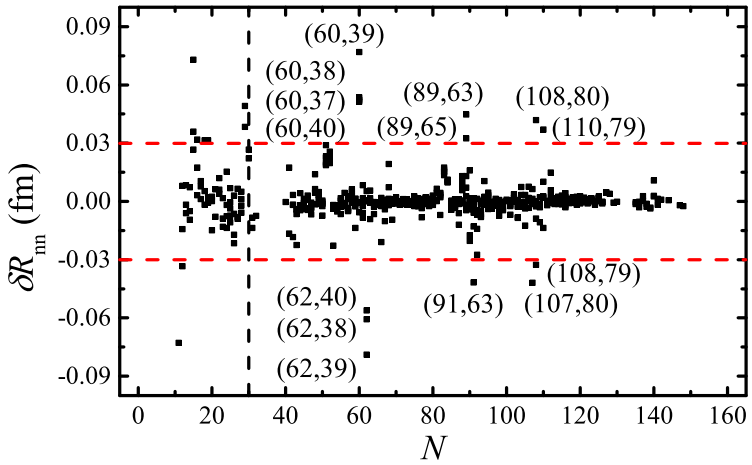

Figure 10. $\delta R_{\rm nn}$ versus N for $N > 10$. The red dash lines correspond to $\delta R_{\rm nn} = \pm 0.03$ fm. For $N, Z > 30$, nuclei (N, Z) with absolute values of $\delta R_{\rm nn} > 0.03$ fm are labeled.

The nuclei (N, Z) with $|\delta R_{\rm nn}| > 0.03$ fm are labeled in Figure 10, and these anomalies can be divided into three regions: (1) $Z = 37 \sim 40$ and $N = 60$ or 62; (2) $Z = 63$ or 65 and $N = 89$ or 91; (3) $Z = 79$, $N = 108$ or 110, and $Z = 80$, $N = 107$ or 108 [42]. These large deviations of $\delta R_{\rm nn}$ are also consistent with the $(\alpha N'_{\rm n} + N'_{\rm p})$ relation for R, as discussed in Section 2.2 [42].

The anomalies in region 3 of Figure 10 are the same as those in Figure 6d. For the other two regions, Figure 11 is plotted to explain those anomalies. Obvious gaps shown in Figure 11a,b lead to those anomalies of regions 1 and 2 of Figure 10, respectively [42].

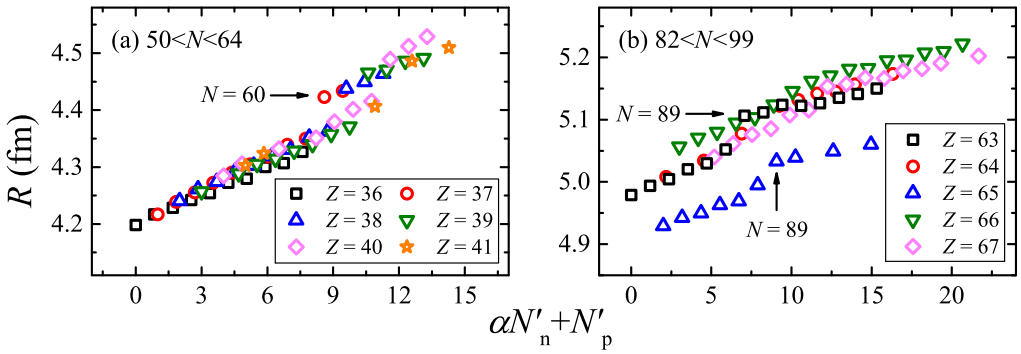

Figure 11. Nuclear charge radii R [43,44] versus $(\alpha N'_{\rm n} + N'_{\rm p})$. Different symbols are used to label the chains of isotopes. The parameter α is 0.844 for panel (**a**) and 1.178 for panel (**b**).

The sudden increase in R at $N = 60$ shown in Figure 11a corresponds to the phase transition at $N = 60$, $Z \sim 40$ (as discussed above in Figure 6b in Section 2.2). The gap in Figure 11b is influenced by the $Z = 64$ subshell [45].

3. Conclusions

In this paper, three kinds of local relations that can reflect many nuclear structure evolutions are introduced, and some results of these models can be verified with each other.

The new magic numbers and Wigner effect can be reflected from $\delta V_{\rm nn}$ and $\delta V_{\rm pp}$. The phase transition at $Z \sim 40$ and $N = 60$ is shown in the $(\alpha N'_{\rm n} + N'_{\rm p})$ relation, and $\delta R_{\rm nn}$, $\delta V_{\rm nn}$ relation. The subshell at $Z = 40$ and $N < 60$ causes a part of the anomalies in $\delta V_{\rm pp}$. The $N_{\rm p}N_{\rm n}$ scheme of e_2, $\delta V_{\rm nn}$, $\delta R_{\rm nn}$ and the $(\alpha N'_{\rm n} + N'_{\rm p})$ relation of R and Q_α show abnormalities at the $Z = 64$ subshell.

The shape coexistence in the region of nuclei with $Z = 76 \sim 81$ and $N \sim 104$ can be given by the e_2 in both the $N_{\rm p}N_{\rm n}$ scheme and the P factor plot, the $E_{2_1^+}$, $E_{4_1^+}$, $E_{6_1^+}$ in the P factor plot, and the $(\alpha N'_{\rm n} + N'_{\rm p})$ relation and the $\delta R_{\rm nn}$ relation for nuclear charge radii R.

In addition, anomalies of nuclei with $66 < Z < 71$ and $82 < N < 88$ arise in the P factor plot of $E_{2_1^+}$, $E_{4_1^+}$, $E_{6_1^+}$, as well as the $(\alpha N'_{\rm n} + N'_{\rm p})$ relation of R and Q_α, and anomalies of $Z = 83$ isotopes arise in both the $(\alpha N'_{\rm n} + N'_{\rm p})$ relations of R and Q_α. The reason for these anomalies is still unknown and should be studied further.

Author Contributions: Conceptualization, M.B.; methodology, M.B.; validation, M.B. and Q.W.; formal analysis, M.B. and Q.W.; investigation, M.B.; data curation, M.B. and Q.W.; writing—original draft preparation, M.B.; writing—review and editing, M.B.; visualization, M.B. and Q.W.; supervision, M.B. All authors have read and agreed to the published version of the manuscript.

Funding: This research was funded by the National Natural Science Foundation of China, grant number 11905130, and Shanghai Sailing Program, grant number 19YF1434200.

Data Availability Statement: Data is contained within the article.

Conflicts of Interest: The authors declare no conflict of interest.

References

1. Bartlett, J.H. Nuclear Structure. *Nature* **1932**, *130*, 165. [CrossRef]
2. Bartlett, J.H. Structure of Atomic Nuclei. *Phys. Rev.* **1932**, *41*, 370–371. [CrossRef]
3. Bartlett, J.H. Structure of Atomic Nuclei. II. *Phys. Rev.* **1932**, *42*, 145–146. [CrossRef]
4. Elsasser, W.M. Sur le principe de Pauli dans les noyaux. *J. Phys. Radium* **1933**, *4*, 549–556. [CrossRef]
5. Elsasser, W.M. Sur le principe de Pauli dans les noyaux—II. *J. Phys. Radium* **1934**, *5*, 389–397. [CrossRef]
6. Elsasser, W.M. Sur le principe de Pauli dans les noyaux—III. *J. Phys. Radium* **1934**, *5*, 635–639. [CrossRef]
7. Mayer, M.G. On Closed Shells in Nuclei. *Phys. Rev.* **1948**, *74*, 235–239. [CrossRef]
8. Mayer, M.G. On Closed Shells in Nuclei. II. *Phys. Rev.* **1949**, *75*, 1969–1970. [CrossRef]
9. Mayer, M.G. Nuclear Configurations in the Spin-Orbit Coupling Model. I. Empirical Evidence. *Phys. Rev.* **1950**, *78*, 16–21. [CrossRef]
10. Haxel, O.; Jensen, J.H.D.; Sueß, H.E. Zur Interpretation der ausgezeichneten Nucleonenzahlen im Bau der Atomkerne. *Naturwissenschaften* **1948**, *35*, 376. [CrossRef]
11. Sueß, H.E.; Haxel, O.; Jensen, J.H.D. Zur Interpretation der ausgezeichneten Nucleonenzahlen im Bau der Atomkerne. *Naturwissenschaften* **1949**, *36*, 153–155. [CrossRef]
12. Jensen, J.H.D.; Sueß, H.E.; Haxel, O. Modellmäßige Deutung der ausgezeichneten Nucleonenzahlen im Kernbau. *Naturwissenschaften* **1949**, *36*, 155–156. [CrossRef]
13. Haxel, O.; Jensen, J.H.D.; Sueß, H.E. On the "Magic Numbers" in Nuclear Structure. *Phys. Rev.* **1949**, *75*, 1766. [CrossRef]
14. Haxel, O.; Jensen, J.H.D.; Sueß, H.E. Modellmäßige Deutung der ausgezeichneten Nukleonenzahlen im Kernbau. *Z. Phys.* **1950**, *128*, 295–311. [CrossRef]
15. Mayer, M.G.; Jensen, J.H.D. *Elementary Theory of Nuclear Shell Structure*; John Wiley & Sons Inc.: New York, NY, USA, 1955.
16. de-Shalit, A.; Talmi, I. *Nuclear Shell Theory*; Academic Press Inc.: New York, NY, USA, 1963.
17. Lawson, R.D. *Theory of the Nuclear Shell Model*; Oxford University Press: New York, NY, USA, 1980.
18. Talmi, I. *Simple Models of Complex Nuclei: The Shell Model and Interacting Boson Model*; Harwood Academic Publishers: Chur, Switzerland, 1993.
19. Editing group for future strategies study of nuclear and plasma physics. *Forefronts and Future Strategies of Nuclear Physics and Plasma Physics*; Science Press: Beijing, China, 2017; pp. 121–206. (In Chinese)
20. Kondev, F.G.; Wang, M.; Huang, W.J.; Naimi, S.; Audi, G. The NUBASE2020 evaluation of nuclear physics properties. *Chin. Phys. C* **2021**, *45*, 030001. [CrossRef]
21. Huang, W.J.; Wang, M.; Kondev, F.G.; Audi, G.; Naimi, S. The AME 2020 atomic mass evaluation (I). Evaluation of input data, and adjustment procedures. *Chin. Phys. C* **2021**, *45*, 030002. [CrossRef]
22. Wang, M.; Huang, W.J.; Kondev, F.G.; Audi, G.; Naimi, S. The AME2020 atomic mass evaluation (II). Tables, graphs and references. *Chin. Phys. C* **2021**, *45*, 030003. [CrossRef]
23. Garvey, G.T.; Kelson, I. New Nuclidic Mass Relationship. *Phys. Rev. Lett.* **1966**, *16*, 197–200. [CrossRef]
24. Garvey, G.T.; Gerace, W.J.; Jaffe, R.L.; Talmi, I.; Kelson, I. Set of Nuclear-Mass Relations and a Resultant Mass Table. *Rev. Mod. Phys.* **1966**, *41*, S1–S80. [CrossRef]
25. Gao, Z.C.; Chen, Y.S. Enhancement of the $n-p$ interaction in odd-odd nuclei. *Phys. Rev. C* **1999**, *59*, 735–739.
26. Gao, Z.C.; Chen, Y.S.; Meng, J. Garvey-Kelson Mass Relations and n-p Interaction. *Chin. Phys. Lett.* **2001**, *18*, 1186–1188.
27. Fu, G.J.; Jiang, H.; Zhao, Y.M.; Pittel, S.; Arima, A. Nuclear binding energies and empirical proton-neutron interactions. *Phys. Rev. C* **2010**, *82*, 034304. [CrossRef]
28. Jiang, H.; Fu, G.J.; Zhao, Y.M.; Arima, A. Nuclear mass relations based on systematics of proton-neutron interactions. *Phys. Rev. C* **2010**, *82*, 054317. [CrossRef]
29. Fu, G.J.; Lei, Y.; Jiang, H.; Zhao, Y.M.; Sun, B.; Arima, A. Description and evaluation of nuclear masses based on residual proton-neutron interactions. *Phys. Rev. C* **2011**, *84*, 034311. [CrossRef]
30. Jiang, H.; Fu, G.J.; Sun, B.; Liu, M.; Wang, N.; Wang, M.; Ma, Y.G.; Lin, C.J.; Zhao, Y.M.; Zhang, Y.H.; et al. Predictions of unknown masses and their applications. *Phys. Rev. C* **2012**, *85*, 054303. [CrossRef]
31. Casten, R.F. N_pN_n systematics in heavy nuclei. *Nucl. Phys. A* **1985**, *443*, 1–28. [CrossRef]
32. Casten, R.F.; Zamfir, N.V. The evolution of nuclear structure: The N_pN_n scheme and related correlations. *J. Phys. G Nucl. Part. Phys.* **1996**, *22*, 1521–1552. [CrossRef]
33. Casten, R.F. *Nuclear Structure from a Simple Perspective*, 2nd ed.; Oxford University Press: New York, NY, USA, 2000.
34. Zhao, Y.M.; Casten, R.F.; Arima, A. Generalization of the N_pN_n Scheme and the Structure of the Valence Space. *Phys. Rev. Lett.* **2000**, *85*, 720–723. [CrossRef] [PubMed]
35. Zhao, Y.M.; Arima, A. Generalization of the N_pN_n scheme to nonyrast levels of even-even nuclei. *Phys. Rev. C* **2003**, *68*, 017301. [CrossRef]
36. Casten, R.F. Possible Unified Interpretation of Heavy Nuclei. *Phys. Rev. Lett.* **1985**, *54*, 1991–1994. [CrossRef]
37. Casten, R.F.; Brenner, D.S.; Haustein, P.E. Valence p-n interactions and the development of collectivity in heavy nuclei. *Phys. Rev. Lett.* **1987**, *58*, 658–661. [CrossRef]
38. Möller, P.; Nix, J.R.; Myers, W.D.; Swiatecki, W.J. Nuclear Ground-State Masses and Deformations. *At. Data Nucl. Data Tables* **1995**, *59*, 185–381. [CrossRef]

39. Sakai, M. Quasi-bands in even-even nuclei. *At. Data Nucl. Data Tables* **1984**, *31*, 399–432. [CrossRef]
40. National Nuclear Data Center. Available online: https://www.nndc.bnl.gov/ (accessed on 27 September 2021). [CrossRef]
41. Zhao, Y.M.; Arima, A.; Casten, R.F. Systematics of nuclear deformation in large regions. *Phys. Rev. C* **2001**, *63*, 067302. [CrossRef]
42. Bao, M.; Zong, Y.Y.; Zhao, Y.M.; Arima, A. Local relations of nuclear charge radii. *Phys. Rev. C* **2020**, *102*, 014306.
43. Angeli, I.; Marinova, K.P. Table of experimental nuclear ground state charge radii: An update. *At. Data Nucl. Data Tables* **2013**, *99*, 69–95. [CrossRef]
44. The Table of Experimental Nuclear Charge Radii. Available online: https://www-nds.iaea.org/radii/ (accessed on 29 September 2021). [CrossRef]
45. Fu, G.J.; Bao, M.; He, Z.; Jiang, H.; Zhao, Y.M.; Arima, A. Pairing interactions and one-nucleon separation energies. *Phys. Rev. C* **2012**, *86*, 054303. [CrossRef]
46. Rowe, D.J.; Wood, J.L. *Fundamentals of Nuclear Models: Foundational Models*; World Scientific Publishing Company: Singapore, 2010; pp. 41–44. [CrossRef]
47. Jia, J.; Qian, Y.; Ren, Z. Systematics of α-decay energies in the valence correlation scheme. *Phys. Rev. C* **2021**, *103*, 024314. [CrossRef]
48. Casten, R.F. A simple approach to nuclear transition regions. *Phys. Lett. B* **1985**, *152*, 145–150. [CrossRef]
49. Ogawa, M.; Broda, R.; Zell, K.; Daly, P.J.; Kleinheinz, P. Lowest 2^+ State in $^{146}_{64}Gd_{82}$ and the Energy Gap at $Z = 64$. *Phys. Rev. Lett.* **1978**, *41*, 289–292.
50. Casten, R.F.; Warner, D.D.; Brenner, D.S.; Gill, R.L. Relation between the $Z = 64$ Shell Closure and the Onset of Deformation at $N = 88$–90. *Phys. Rev. Lett.* **1981**, *47*, 1433–1436. [CrossRef]
51. Zamfir, N.V.; Casten, R.F. Nonpairing like-nucleon valence residual interactions. *Phys. Rev. C* **1991**, *43*, 2879–2882. [CrossRef]
52. Casten, R.F.; Zamfir, N.V. Evolution of pre-collective nuclei: Structural signatures near the drip lines. *Phys. Scr.* **1995**, *T56*, 47–57.
53. Ozawa, A.; Kobayashi, T.; Suzuki, T.; Yoshida, K.; Tanihata, I. New Magic Number, $N = 16$, near the Neutron Drip Line. *Phys. Rev. Lett.* **2000**, *84*, 5493–5495. [CrossRef]
54. Gupta, R.K.; Balasubramaniam, M.; Kumar, S.; Patra, S.K.; Münzenberg, G.; Greiner, W. Magic numbers in exotic light nuclei near drip lines. *J. Phys. G Nucl. Part. Phys.* **2006**, *32*, 565–571. [CrossRef]
55. Federman, P.; Pittel, S. Unified shell-model description of nuclear deformation. *Phys. Rev. C* **1979**, *20*, 820–829. [CrossRef]
56. Tabor, S.L. Collective systematics in the mass 80 region. *Phys. Rev. C* **1986**, *34*, 311–316. [CrossRef]